J. Fluid Mech. (2002), *vol.* 454, *pp.* 263–286.
DOI: 10.1017/S0022112001007145 Printed in the United Kingdom

Slip velocity and lift

By D. D. JOSEPH AND D. OCANDO

Department of Aerospace Engineering and Mechanics and the Minnesota Supercomputer Institute, University of Minnesota, Minneapolis, MN 55455, USA

(Received 15 November 2000 and in revised form 3 August 2001)

The lift force on a circular particle in plane Poiseuille flow perpendicular to gravity is studied by direct numerical simulation. The angular slip velocity $\Omega_s = \Omega_p + \frac{1}{2}\dot{\gamma}$, where $-\frac{1}{2}\dot{\gamma}$ is the angular velocity of the fluid at a point where the shear rate is $\dot{\gamma}$ and Ω_p is the angular velocity of the particle, is always positive at an equilibrium position at which the hydrodynamic lift balances the buoyant weight. The particle migrates to its equilibrium position and adjusts Ω_p so that $\Omega_s > 0$ is nearly zero because $\Omega_p \approx -\frac{1}{2}\dot{\gamma}$. No matter where the particle is placed, it drifts to an equilibrium position with a unique, slightly positive equilibrium angular slip velocity. The angular slip velocity discrepancy defined as the difference between the angular slip velocity of a migrating particle and the angular slip velocity at its equilibrium position is positive below the position of equilibrium and negative above it. This discrepancy is the quantity that changes sign above and below the equilibrium position for neutrally buoyant particles, and also above and below the lower equilibrium position for heavy particles. The existence and properties of unstable positions of equilibrium due to newly identified turning-point transitions and those near the centreline are discussed.

The long particle model of Choi & Joseph (2001) that gives rise to an explicit formula for the particle velocity and the velocity profile across the channel through the centreline of the particle is modified to include the effect of the rotation of the particle. In view of the simplicity of the model, the explicit formula for U_p and the velocity profile are in surprisingly good agreement with simulation values. The value of the Poiseuille flow velocity at the point at the particle's centre when the particle is absent is always larger than the particle velocity; the slip velocity is positive at steady flow.

1. Introduction

The experiments of Segré & Silberberg (1961, 1962) have influenced the fluid mechanics studies of migration and lift. They studied the migration of dilute suspensions of neutrally buoyant spheres in pipe flows at Reynolds numbers between 2 and 700. The particles migrate away from the wall and centreline and accumulate at 0.6 of a pipe radius.

The lift on heavier than liquid particles is also influenced by the factors that determine the equilibrium position of neutrally buoyant particles. The heavy particles must reach an equilibrium that balances the hydrodynamic lift and buoyant weight. If the buoyant weight is very small, the equilibrium position of the particles will be close to the value for the neutrally buoyant case. The effect of increasing the weight is to lower the equilibrium position whose zero is established for the case of zero buoyant weight.

Analysis of the lift of a neutrally buoyant heavy and light particles may be framed

in a uniform way by looking for the equilibrium positions of particles evolving to steady flow under the action of shear from the Poiseuille flow as positions at which the buoyant lift, the lift minus the buoyant weight, vanishes. Loosely speaking, these equilibrium positions can be regarded as generalized Segré–Silberberg radii.

Most attempts to explain the Segré–Silberberg effects have been based on linearized low-Reynolds-number hydrodynamics. Possibly the most famous of these attempts is due to Saffman (1965), who found that the lift on a sphere in a linear shear flow is given by

$$L = 6.46\eta a^2 U_s(\dot{\gamma}/\nu)^{1/2} + \text{lower-order terms}, \tag{1.1}$$

where $U_s = U_f - U_p$ is the slip velocity, U_f is the fluid velocity and U_p is the particle velocity, a is the sphere radius, $\nu = \eta/\rho_f$, η is the fluid viscosity, ρ_f is the fluid density and $\dot{\gamma}$ is the shear rate. The lower-order terms are

$$-U_s a^3 \rho_f [\pi\Omega_s - (\pi - \tfrac{22}{8})\tfrac{1}{2}\dot{\gamma}], \tag{1.2}$$

where

$$\Omega_s = \Omega_p + \tfrac{1}{2}\dot{\gamma} \tag{1.3}$$

is the angular slip velocity and Ω_p is the particle angular velocity. Slip velocities are important because shear gradients define the local environment against which particle translations are measured. There are a number of formulae like Saffman's that are in the form of U_s multiplied by a factor, which can be identified as a density multiplied by a circulation as in the famous formula $\rho U\Gamma$ for aerodynamic lift. A review of such formulae can be found in McLaughlin (1991).

Formulae like Saffman's cannot explain Segré–Silberberg's observations, which require migration away from both the wall and the centre. There is nothing in these formulae to account for the migration reversal near 0.6 of a radius. Moreover, the slip velocity U_s, the angular slip velocity Ω_s, the particle velocity and the particle angular velocity, which are functionals of the solution are prescribed quantities in these formulae.

The fluid motion drives the lift on a free body in shear flow; no external forces or torques are applied. If there is no shear, there is no lift. In Poiseuille flow, there is not only a shear, but a shear gradient. Gradients of shear (curvature) produce lateral forces. At the centreline of a Poiseuille flow, the shear vanishes, but the shear gradient does not. To understand the Segré–Silberberg effect, it is necessary to know that the curvature of the velocity profile at the centre of the Poiseuille flow makes the centre of the channel an unstable position of equilibrium. A particle at the centre of the channel or pipe will be driven by shear gradients toward the wall; a particle near the wall will lag the fluid and be driven away from the wall. An equilibrium radius away from the centre and wall must exist.

Ho & Leal (1974) were the first to combine these effects in an analysis of the motion of a neutrally buoyant sphere rotating freely between plane walls so closely spaced that the inertial lift can be obtained by perturbing Stokes flow with inertia. They treated wall effects by a method of reflection and found an equilibrium position at 0.69 from the centre. Vasseur & Cox (1976) used another method to treat wall effects and their results are close to Ho & Leal's near the centreline, but rather different from those of Ho & Leal near the wall. Feng, Hu & Joseph (1994) studied the motion of solid circles in plane Poiseuille flow by direct numerical simulation (DNS). The circle migrates to the 0.6 of a radius equilibrium position. They compared their two-dimensional results with those of Ho & Leal and Vasseur & Cox. Schonberg & Hinch (1989) analysed the lift on a neutrally buoyant small sphere in a plane Poiseuille

flow using matched asymptotic methods. The same problem for neutrally buoyant and non-neutrally buoyant small spheres has been studied by Asmolov (1999) using asymptotic methods. The linearized analysis given so far takes the effect of inertia $(\boldsymbol{u}\cdot\nabla)\boldsymbol{u}$ into account only in an Oseen linear system; the comparison of the results of these analyses with experiments is far from perfect. The analysis is heavy and explicit formulae for lift are not obtained.

Recent three-dimensional numerical studies by Kurose & Komori (1999) and Cherukat, McLaughlin & Dandy (1999) focus on lift and drag on a stationary sphere in a linear (not Poiseuille) shear flow. Issues related to equilibrium positions do not arise in these studies. The recent DNS study of migration of a single liquid drop in Poiseuille flow by Mortazavi & Tryggvason (2000) is relevant to our work. They carried out mainly two-dimensional simulations and a few three-dimensional studies at $Re = 10$ using coarse grids. Though their methods have not been used for solids, the migration to intermediate equilibrium positions is a shared feature. Their results showed that the equilibrium position of the drops is close to the two-dimensional predictions, and the two- and three-dimensional results were similar in other respects.

This paper approaches the problem of migration and lift in a different way. We have used DNS as a diagnostic tool to analyse the role of the slip velocity and the angular slip velocity on migration and lift. In this way, we are able to establish a simple picture of lift and migration that, in particular, clarifies the role of the angular slip velocity, and is not restricted to low Reynolds numbers. We also use DNS to formulate and validate a long particle model that gives a very good, completely explicit analytical approximation to the velocity and slip velocity of circular particles. Our analysis is carried out in two dimensions, but should apply in principle to three dimensions, which is at present under study.†

2. Mechanism for lift

First, we can look at formulae in a fluid without viscosity for which viscous drag is impossible. The most famous formula for lift on a body of arbitrary shape moving forward with velocity U in a potential flow with circulation Γ was given by

$$L' = \rho U \Gamma \tag{2.1}$$

where ρ is the fluid density and L' is the lift per unit length.

The lift on circular cylinder of radius a is of special interest. A viscous potential flow solution for a stationary cylinder rotating with angular velocity Ω which satisfies the no-slip boundary condition is given by

$$\boldsymbol{u}(r) = \boldsymbol{e}_\theta \Omega a^2/r, \quad \boldsymbol{u}(a) = \boldsymbol{e}_\theta \Omega a. \tag{2.2}$$

The circulation for this viscous potential flow is

$$\Gamma = \oint \boldsymbol{u}\cdot \mathrm{d}\boldsymbol{x} = 2\pi\Omega a^2. \tag{2.3}$$

† A referee called our attention to a paper by Zhao, Sharp & James (1998) on transverse lift on a free circular particle in steady flow in a channel. The three main results of our paper, (i) the stability of intermediate equilibrium positions arising from the dynamic resolution of the initial value problem, (ii) the long body model, and (iii) the explanation of the Segré–Silberberg effect by identification of the slip quantity, which changes the sign of the lift across the equilibrium position, are not touched in their paper. Our results and theirs agree where they overlap.

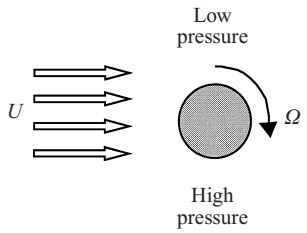

FIGURE 1. The lift per unit length $L' = 2\pi\rho a^2 U\Omega$ on a cylinder of radius a moving forward at speed U and rotating with angular velocity Ω in such a way as to reduce the velocity at the bottom and add at the top.

When this rotating cylinder moves forward, it generates a lift L' per unit length

$$L' = 2\pi\rho a^2 U\Omega. \tag{2.4}$$

The direction of the lift can be determined by noting that the velocity due to rotation adds to the forward motion of the cylinder at the top or bottom of the rotating cylinder according to the directions of Ω and U. In figure 1, the velocity is smaller on the bottom of the cylinder; by the Bernoulli equation, the pressure is greater there and it pushes the cylinder up.

Another formula for the lift on a particle in an inviscid fluid in which uniform motion is perturbed by a weak shear was derived by Auton (1987) and a more recent satisfying derivation of the same result was given by Drew & Passman (1999). They find that in a plane flow

$$\boldsymbol{L} = \tfrac{4}{3}\pi a^3 \rho\Omega_f U_s \boldsymbol{e}_y, \tag{2.5}$$

where

$$2\Omega_f = -\dot{\gamma} = -\frac{\mathrm{d}u}{\mathrm{d}y}.$$

If $\mathrm{d}u/\mathrm{d}y > 0$, the sphere is lifted against gravity when the slip velocity U_s is positive; if U_s is negative, the sphere will fall. Particles which lag the fluid migrate to streamlines with faster flow, particles which lead the fluid migrate to streamlines with slower flow.

There are striking differences between (2.5) and (2.4); first, (2.4) depends on the angular velocity of the particle, but (2.5) depends on the angular velocity of the fluid. Both formulae leave the slip velocity undetermined, U_s appears in (2.5) because of the shear, in (2.4), $U_f = 0$. The slip velocities have to be prescribed in these theories because the particle velocity is not determined by viscous drag. Similarly, the angular velocity of the particle cannot arise from torques arising from viscous shears. The effects of particle rotation cannot be obtained by the method of Auton (1987).

The lift formula $\rho U\Gamma$ captures the essence of the mechanism in which the motion of the particle relative to the fluid is such as to increase the pressure on the side of the particle as it moves forward.

The lift on a spherical or circular particle in a shear flow is different; there is no exterior agent to move and rotate the freely moving particle. Instead, the particle is impelled forward and rotated by the shear flow. Previous theoretical studies and our simulations show that the relevant velocity is the slip velocity and the relevant circulation is proportional to an angular slip velocity discrepancy $\Gamma_s \propto \Omega_s - \Omega_{se}$ where Ω_{se} is the angular slip velocity in equilibrium (steady flow with zero buoyant lift) and

$$L' = CU_s\Gamma_s, \tag{2.6}$$

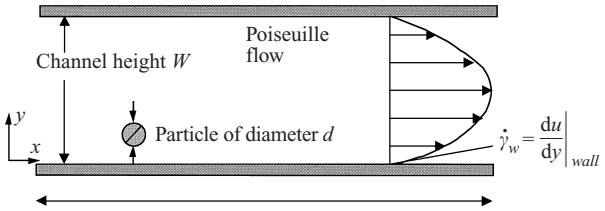

FIGURE 2. Migration and lift of a single particle in a plane Poiseuille flow.

where C is a to-be-determined function of fluid and flow parameters. This conclusion will be established in the sequel. For now we simply note that in our simulations, the angular slip velocity discrepancy $\Omega_s - \Omega_{se} < 0$ when the cylinder is above the equilibrium (Segré–Silberberg) position and $\Omega_s - \Omega_{se} > 0$ when it is below the equilibrium (figure 10).

3. Governing equations, problem formulation

The simulation method used in this paper is described in Joseph (2000), Choi & Joseph (2001) and Patankar *et al.* (2001). A circular particle of diameter d is placed in a plane Poiseuille flow in a channel of height W where it moves forward in the direction x and migrates up or down in the direction y under the action of hydrodynamic forces (figure 2).

The undisturbed Poiseuille flow (no particle) is given by

$$\left.\begin{aligned} u(y) &= 4u_m \frac{y}{W}\left(1-\frac{y}{W}\right), \quad \dot{\gamma} = \frac{du}{dy}, \\ u_m &= u\left(\frac{W}{2}\right) = \frac{W^2\bar{p}}{8\eta}, \qquad \dot{\gamma}_w = \frac{4u_m}{W} = \frac{W^2\bar{p}}{2\eta}. \end{aligned}\right\} \tag{3.1}$$

Flows are indexed by a Reynolds number

$$R = \dot{\gamma}_w d^2/v, \quad v = \eta/\rho_f \tag{3.2}$$

based on the wall shear rate $\dot{\gamma}_w$.

3.1. *Governing equations*

The fluid–particle system is governed by the Navier–Stokes equations for the fluid and Newton's equations for rigid-body motions. The fluid satisfies

$$\rho_f\left[\frac{\partial \boldsymbol{u}}{\partial t} + \boldsymbol{u}\cdot\nabla\boldsymbol{u}\right] = -\nabla p + \eta\nabla^2\boldsymbol{u} + \bar{p}\boldsymbol{e}_x, \tag{3.3}$$

where $\bar{p}$ is the constant pressure gradient. The particle satisfies Newton's equations of motion: The motion $\boldsymbol{U}_p$ of the mass centre is governed by

$$\rho_p\frac{d\boldsymbol{U}_p}{dt} = -(\rho_p-\rho_f)g\boldsymbol{e}_y + \bar{p}\boldsymbol{e}_x + \frac{1}{V_p}\oint\{-p\mathbf{1} + 2\eta\boldsymbol{D}[\boldsymbol{u}]\}\cdot\boldsymbol{n}\,d\Gamma, \tag{3.4}$$

where $V_p = \pi a^2$ is the volume of the particle and $(-p\mathbf{1} + 2\eta\boldsymbol{D}[\boldsymbol{u}])\cdot\boldsymbol{n}$ is the stress on the surface Γ of the particle that is a circle of radius $a = \frac{1}{2}d$ and

$$\oint(\cdot)\,d\Gamma = a\int_0^{2\pi}(\cdot)\,d\theta. \tag{3.5}$$

The angular velocity around the mass centre at $\boldsymbol{x} = \boldsymbol{X}$ is governed by

$$I\frac{\mathrm{d}\boldsymbol{\Omega}}{\mathrm{d}t} = \oint (\boldsymbol{x} - \boldsymbol{X}) \wedge [(-p\mathbf{1} + 2\eta \boldsymbol{D}[\boldsymbol{u}]) \cdot \boldsymbol{n}]\, \mathrm{d}\Gamma, \tag{3.6}$$

where $I = \rho_p \pi a^4$ is the moment of inertia.

In steady (equilibrium) flow the forward motion of the particle is given by

$$\bar{p} + \frac{1}{\pi a}\int_0^{2\pi} \boldsymbol{e}_x \cdot \{-p\mathbf{1} + 2\eta \boldsymbol{D}[\boldsymbol{u}]\} \cdot \boldsymbol{e}_r\, \mathrm{d}\theta = 0. \tag{3.7}$$

The pressure gradient force on the particle is balanced by the resultant of the stress traction vector. The long particle model discussed by Joseph (2000), Choi & Joseph (2001) and here in § 4 is a realization of (3.7).

3.2. *Dimensionless parameters*

A dimensionless form of these equations was given in Joseph (2000), Choi & Joseph (2001) and Patankar *et al.* (2001). The parameters at play are the channel width diameter ratio W/d which is fixed at 12 here, the density ratio ρ_p/ρ_f and the gravity Reynolds number

$$R_G = \rho_f(\rho_p - \rho_f) g d^3/\eta^2. \tag{3.8}$$

Thus, there are four dimensionless parameters at play; the density ratio parameter ρ_p/ρ_f does not enter when the accelerations vanish, reducing the number of parameters to three. The case $W/d = 12$ used here is representative of the asymptotic condition $W/d > 12$ (Patankar *et al.* 2001), only R and R_G enter. Here, we compute for $\eta = 1.0$ poise, $\rho_f = 1\,\mathrm{g\,cm^{-3}}$, $g = 980\,\mathrm{cm\,s^{-2}}$, $d = 1\,\mathrm{cm}$ with $\rho_p/\rho_f = 1$ or $\rho_p/\rho_f = 1.01$. For these two $R_G = 0$ or

$$R_G = 9.8. \tag{3.9}$$

We will work with dimensional variables in CGS units, but we do specify R. Hence, when we compute for $\rho_p = 1.01$ g cm^{-3}, we understand that $R_G = 9.8$. The results at steady flow do not depend on ρ_p/ρ_f so that lift in steady flow results with $\rho_p/\rho_f = 1.01$ are valid when $R_G = 9.8$, independent of ρ_p.

3.3. *Stable and unstable equilibria*

It may be helpful to frame the problem in terms of the lift-off of a heavier than liquid particle. A qualitative description of the levitation to equilibrium particle can be framed as follows: the particle rests on the bottom wall when there is no flow. As the pressure gradient is increased, the circular particle starts to slide and roll. At critical speed, the particle lifts and finally rises to a height in which the lift balances the buoyant weight. It then moves forward freely under zero net force and torque; the particle does not accelerate. After the particle lifts off, it rises to the equilibrium height y_e where the lift balances the buoyant weight. The slip velocity $U_f - U_p$ and angular slip velocity $\Omega_p - \Omega_f = \Omega_p - \frac{1}{2}\dot{\gamma}$ can be computed during migration and at equilibrium.

For certain Reynolds numbers, heavier than liquid particles undergo 'turning-point transitions' leading to multiple equilibrium solutions with different values of y_e, U_{pe} and Ω_{pe} (see figure 3). These transitions do not occur for neutrally buoyant particles; the conditions under which 'turning-point transitions' occur will be the subject of a future paper.

For the present study, it is essential to maintain a sharp distinction between unstable

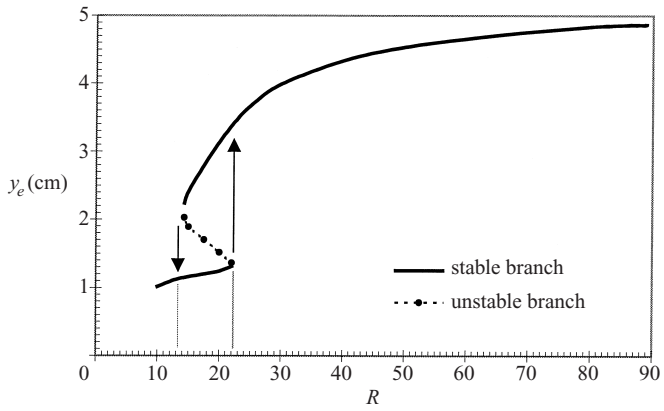

FIGURE 3. (Patankar *et al.* 2001.) Equilibrium height as a function of shear Reynolds number for $\rho_p = 1.01\,\mathrm{g\,cm^{-3}}$. This curve was found first in the dynamic simulations of Choi & Joseph (2001). The turning points and the unstable branch were determined by the method of constrained simulation (see § 4). The solutions are unique for $R < 13$ and $R > 22$; between, there are two stable and one unstable solutions.

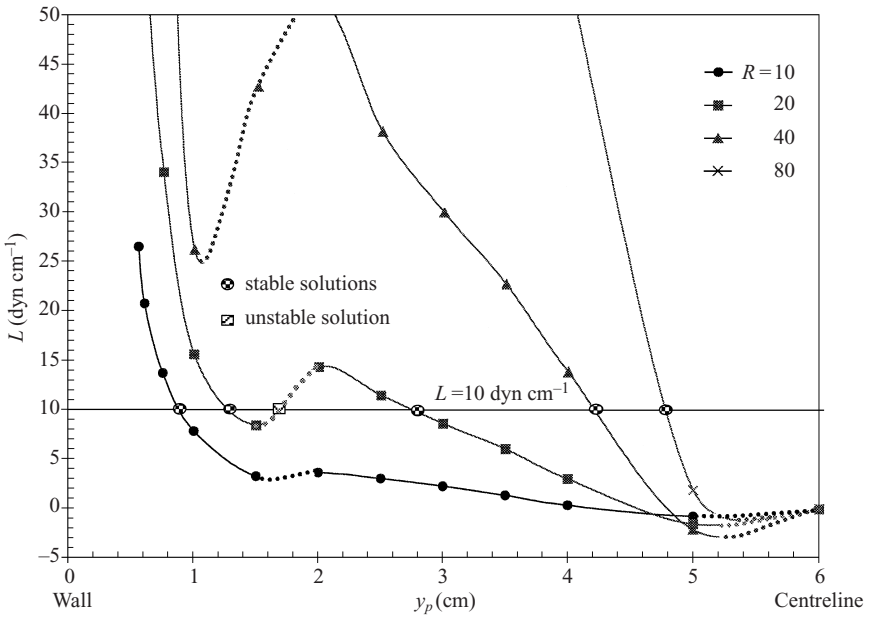

FIGURE 4. Family of lift curves at steady state for different values of R. The lift curves can be anti-symmetrically extended into $6\,\mathrm{cm} < y < 12\,\mathrm{cm}$. The equilibrium points for $R_G = 12.7$ on these lift curves are those satisfying (4.1) for which the hydrodynamic lift balances the buoyant weight. The locus of such equilibrium points y_e *vs.* R are represented in the curve shown in figure 5.

and stable equilibria. The behaviour of particles at unstable equilibria is, in a sense, the opposite of stable equilibria (cf. figures 12 and 13) and there are more subtle differences. We will indicate the unstable equilibria by dotted lines as in figures 4 and 5.

Neutrally buoyant particles are also in a buoyant-weight/lift balance, but both are zero. Freely moving neutrally buoyant particles also migrate to an equilibrium (Segré–Silberberg) position, which is determined by wall effects and shear gradients.

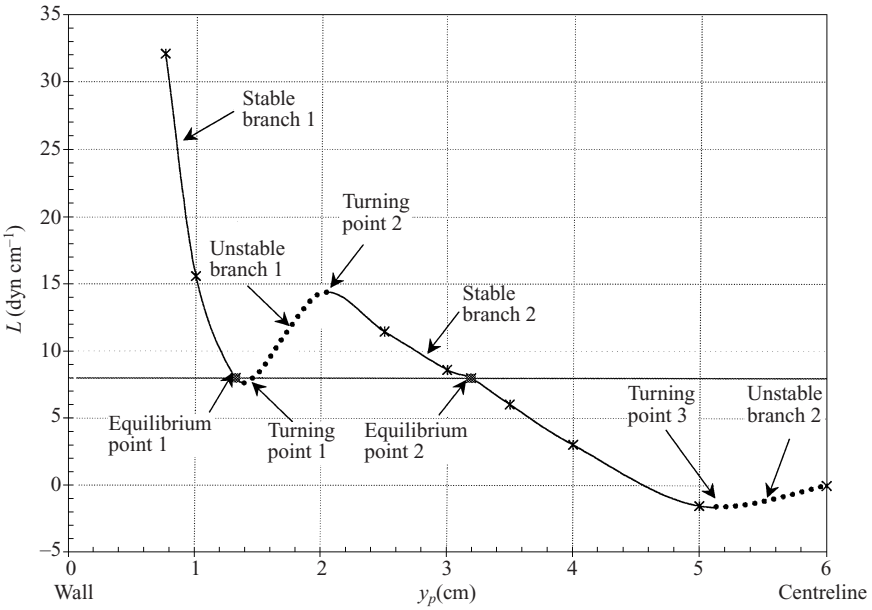

FIGURE 5. Lift *vs.* y for $R = 20$ and $R_G = 9.8$ for the steady forward motion of a circular particle in Poiseuille flow. The equilibrium points are the places where the lift balances the buoyant weight for $\rho_p = 1.01\rho_f$; there are two stable points and one unstable. The picture is anti-symmetric with respect to the centreline and the graph shows that a region near the centre is unstable.

It is very important to frame the analysis of migration and lift relative to the position of equilibrium, a point at which the lift must change its sign.

4. Constrained and unconstrained dynamic simulation

In numerical experiments, we can examine the physical effects one at a time; this cannot be done in real experiments. In a constrained simulation, we let the motion of a particle evolve to steady state while holding some variable fixed; for example, we could require that the angular velocity of the particle is zero and monitor the migration to its equilibrium position, or we could fix the position of the particle and see how the particle velocity, angular velocity and lift L evolve to steady state. The fixed position will be an equilibrium when the lift L balances the buoyant weight $(\rho_p - \rho_f)V_p g = L_e$; that is, when

$$\rho_p = \rho_f + \frac{L_e}{V_p g}. \tag{4.1}$$

For other values of ρ_p the fixed position simulation will evolve to a different steady state, independent of ρ_p/ρ_f multiplying acceleration, in which L is greater or less than L_e.

The method of constrained simulation was used by Patankar *et al.* (2001) to analyse turning-point transitions. The results of such simulations are shown in figure 3. We start a particle from rest at a fixed y and R and let the simulation run to steady flow. At steady flow, we compute L giving the triplet (R, y, L); now varying y at a fixed R we obtain a curve L *vs.* y at a fixed R. A family of such curves for different R is shown in figure 4. The straight line intersecting the curves represents a fixed value

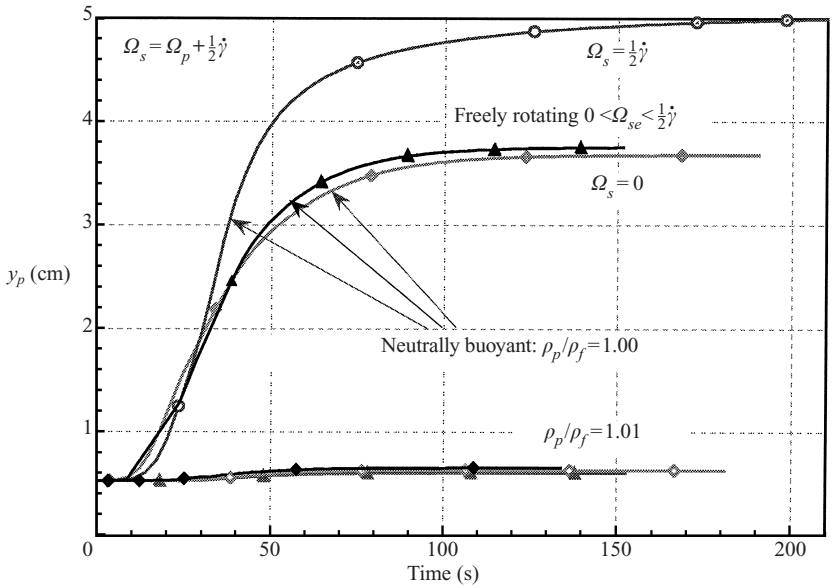

FIGURE 6. Rise *vs.* time for $R = 5.4$. Compare rise of freely rotating and non-rotating particles. Non-rotating particles rise more. A neutrally buoyant, freely rotating particle rises closer to the centreline at $y_p = 6$ cm than the particle for which $\Omega_p = -\frac{1}{2}\dot{\gamma}$; the non-rotating particle rises even more. Models which ignore particle rotation overestimate lift. A yet smaller lift is obtained when the angular slip velocity is entirely suppressed ($\Omega_s = 0$), but the particle does rise. The greater the angular slip velocity, the higher the particle will rise.

of $R_G = 12.7$. There is a value ρ_p given by (4.1) for which L balances the buoyant weight; for all other values of ρ_p, the particles will migrate.

In an unconstrained dynamic simulation, we introduce a circular particle with a prescribed particle velocity U_p and angular velocity Ω_p at a point y_p at the particle centre into a fully developed Poiseuille flow, (3.1). The particle will migrate to an equilibrium position y_e and will attain an equilibrium velocity U_{pe} and angular velocity Ω_{pe}. It is possible to consider migration for different initial conditions; we are computing solutions of initial-value problems. In the study of lift, steady solutions are important because of the absence of complicating effects of particle acceleration.

In a different kind of constrained simulation, we look at the effect on particle migration of controlling the angular velocity of the particle. In figure 6, we plotted the rise to equilibrium of a neutrally buoyant particle for three different values of the angular slip velocity

$$\Omega_s = \Omega_p + \tfrac{1}{2}\dot{\gamma} = \{0,\ \Omega_{se},\ \tfrac{1}{2}\dot{\gamma}\} \tag{4.2}$$

in an unconstrained dynamic simulation. The rise is the greatest when the particle angular velocity $\Omega_p = 0$, and the least when the particle angular velocity is equal to the local rate of rotation $\Omega_p = -\frac{1}{2}\dot{\gamma}$. The rise of a heavier than liquid $\rho_p/\rho_f = 1.01$ circular particle is plotted in figure 6 for Reynolds number $R = \dot{\gamma}_w d^2/\nu = 5.4$ and for $R = 16.2$ in figure 7. The angular slip velocity $\Omega_{se} > 0$ is the equilibrium value that a free circular particle takes in torque-free motion when the angular acceleration vanishes. We call attention to the fact that $\Omega_{se} > 0$ is very small, and at equilibrium

$$|\ \tfrac{1}{2}\dot{\gamma}\ | > |\ \Omega_{pe}\ |, \quad \Omega_{pe} \approx -\tfrac{1}{2}\dot{\gamma}. \tag{4.3}$$

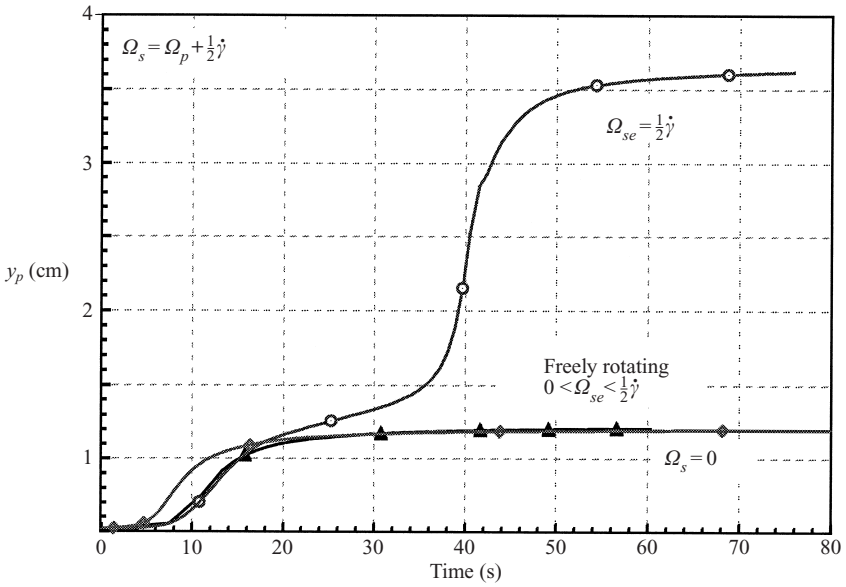

FIGURE 7. Rise *vs.* time for a circular particle $\rho_p/\rho_f = 1.01$ when $R = 16.2$. The rise of the particle is an increasing function of the angular slip velocity in the range $0 \leqslant \Omega_s \leqslant \frac{1}{2}\dot{\gamma}$ and is a maximum when the particle angular velocity is suppressed. The freely rotating particle has a small positive angular slip velocity.

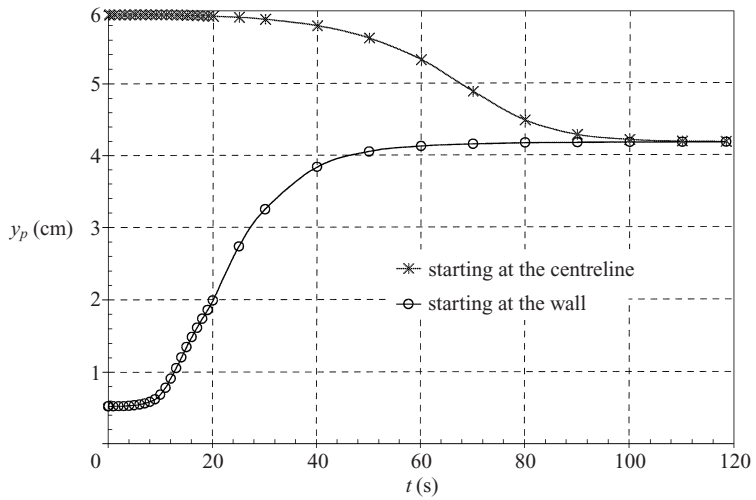

FIGURE 8. Migration of a neutrally buoyant particle in an unconstrained simulation at $R = 10$.

5. Slip velocities, angular slip velocities, and lift for neutrally buoyant circular particles

Multiple equilibrium solutions do not appear at moderate numbers when $\rho_p = \rho_f$, $R_G = 0$; the equilibrium solutions are unique. Figures 8, 9 and 10 show the evolution to equilibrium of a neutrally buoyant particle started at the wall and at the centreline from rest, at $R = 10$. No matter where the particle is released, it will migrate to a unique equilibrium solution $y_e = 4.18$ cm.

In figure 9, we show the evolution of the slip velocity to equilibrium. The slip

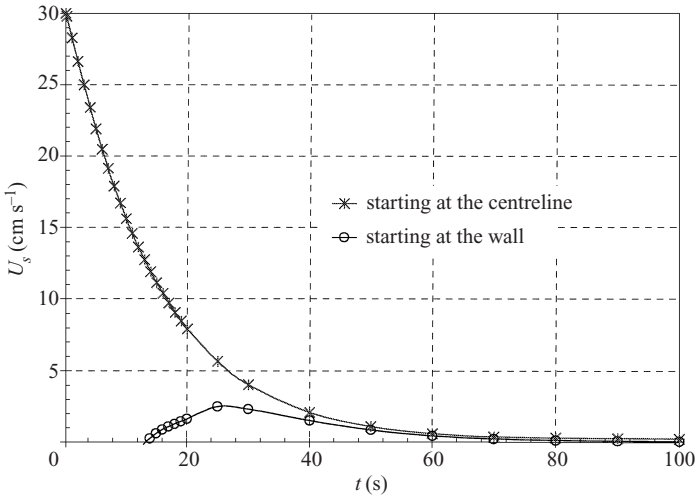

FIGURE 9. Evolution of the slip velocity of the particle whose trajectory is shown in figure 8. The slip velocity evolves to zero through positive values whether the particle is started above or below the centreline. The slip velocity discrepancy $U_s - U_{se} > 0$, $U_{se} = 0.148\,\mathrm{cm\,s^{-1}}$.

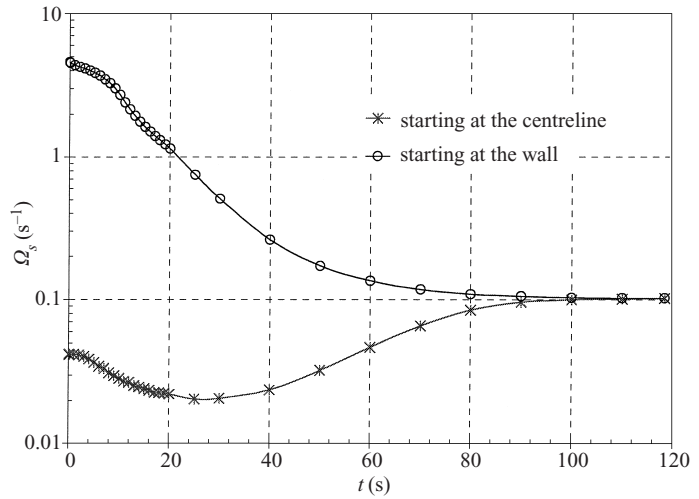

FIGURE 10. Evolution of the angular slip velocity of a neutrally buoyant particle at $R = 10$ to equilibrium (see figure 8). The angular slip velocity function evolves without crossing the equilibrium value. When the angular slip velocity is below the equilibrium value, the particle moves downward. When the angular slip velocity is above the equilibrium value, the particle moves upward.

velocity is positive and, of course, the greatest for a particle released from rest at the centreline.

In figure 10, we show that the angular slip velocity is smaller than its equilibrium value when the particle is above the equilibrium position and is larger than its equilibrium value when it is below the equilibrium position. The angular slip velocity discrepancy,

$$\Omega_s - \Omega_{se}$$

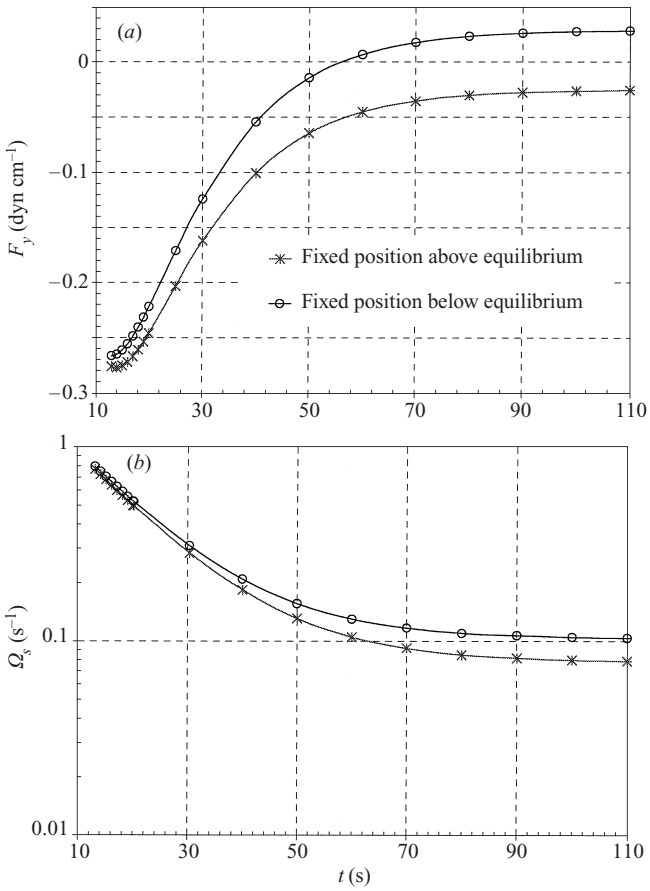

FIGURE 11. (*a*) Lift and (*b*) angular slip velocity in constrained simulations of a particle fixed above and below equilibrium. The sign of the lift correlates perfectly with the sign of the angular slip velocity discrepancy. $R = 10$, $y_p = 4.16$ and 4.19 cm, $y_e = 4.18$ cm.

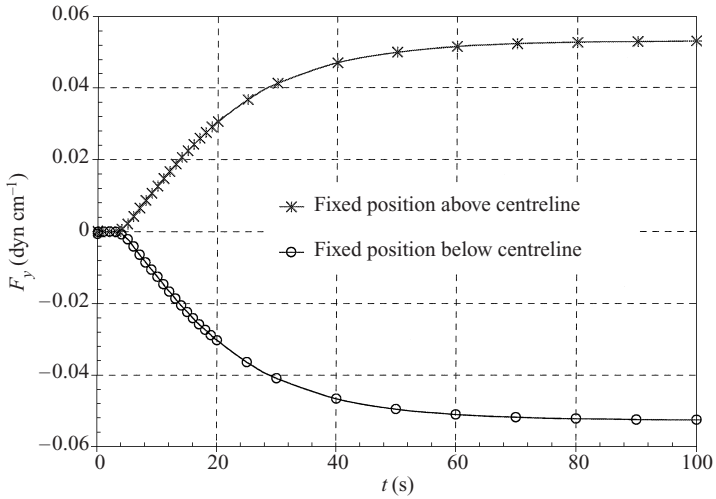

FIGURE 12. Evolution of the lift on a particle at a fixed position at $R = 10$ slightly above, $y_p = 6.05$ cm and below, $y_p = 5.95$ cm, the centreline. The lift pushes the particle away from the centreline.

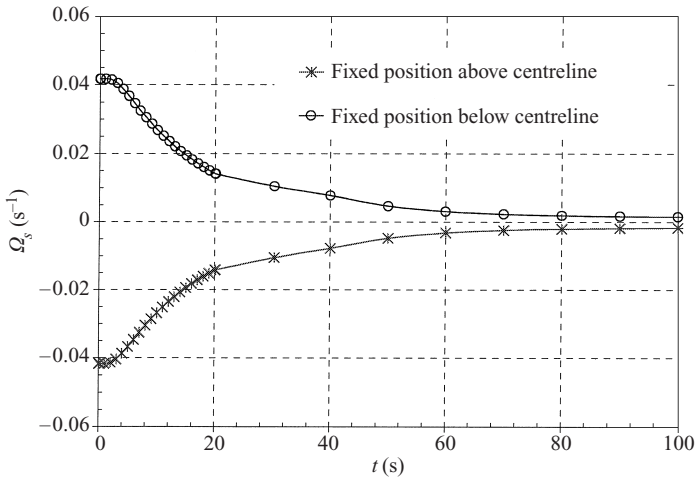

FIGURE 13. Evolution of the angular slip velocity in a constrained simulation for particles at $y_p = 5.95\,\text{cm}$ and $6.05\,\text{cm}$ when $R = 10$. The evolution is to a steady state with the following properties: when the angular slip velocity is below the equilibrium value, the particle moves upward. When the angular slip velocity is above the equilibrium value, the particle moves downward. This behaviour is the opposite of the previous cases, because the previous cases were stable equilibrium positions, and therefore, the force field around them is the opposite.

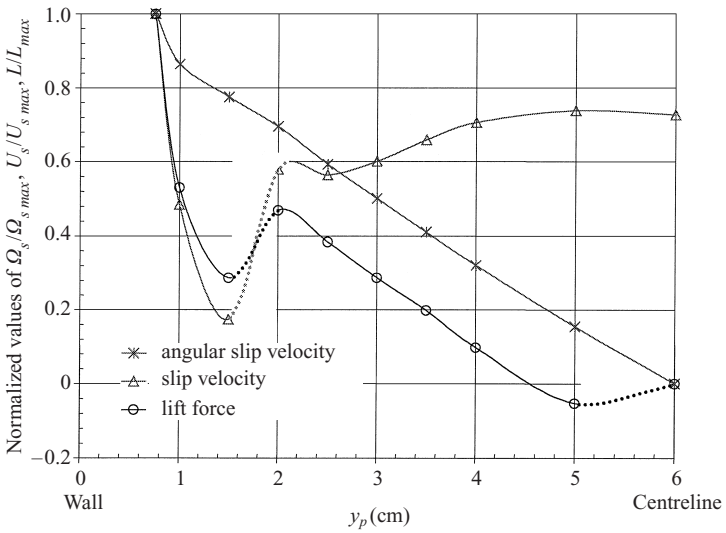

FIGURE 14. Slip velocities and lift for neutrally buoyant particle at $R = 20$. Steady-state relative values for the lift force and the slip velocities. Dotted lines correspond to unstable equilibria. In the region close to the wall, the lift force and the slip velocity have a similar nonlinear behaviour. In the region close to the centreline, the lift force appears to be proportional to the angular slip velocity.

where Ω_{se} is the angular slip velocity at equilibrium, changes sign with the lift across the equilibrium.

In figure 11, we carry out a constrained simulation in which the circular particle is fixed at a position slightly above and slightly below the value of equilibrium. This figure shows that the sign of the angular slip velocity discrepancy changes with the

	y_e (cm)	
ρ_p/ρ_f	Starting at centreline	Starting close to wall
1	4.56	4.56
1.005	3.834	3.834
1.01	3.165	1.323

TABLE 1. Position of equilibrium when $R = 20$.

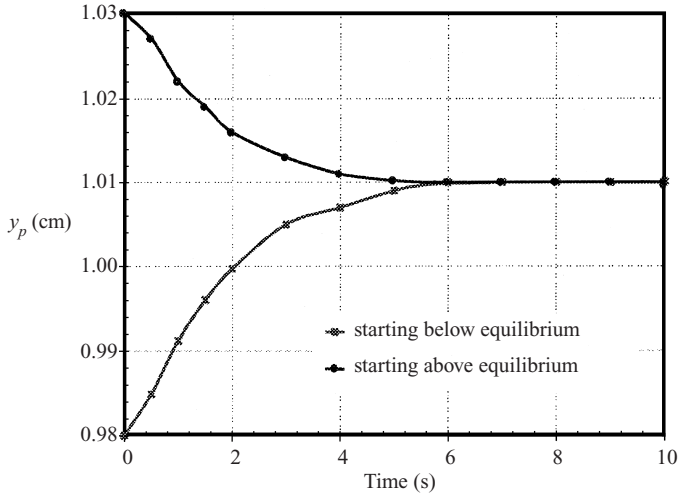

FIGURE 15. Particle height about equilibrium for a heavier than fluid particle ($\rho_p/\rho_f = 1.01$, $R = 10$). The initial condition was the steady-state solution from a constrained simulation at the initial height.

sign of the lift, which is positive for particles below and negative for particles above the equilibrium.

In figures 12 and 13 are shown the evolution of the lift and angular slip velocity, respectively, from constrained simulations at fixed positions slightly above and slightly below the channel centreline.

Figure 13 shows that the angular slip velocity discrepancy is negative when the particle is above the centreline and is positive when it is below the centreline. The discrepancy changes sign in both the stable and unstable case, but the sign of the discrepancy is opposite in the two cases.

In figure 14, we have plotted the resultant constrained dynamical simulation comparing distributions of the normalized slip velocity, the angular slip velocity and lift for a neutrally buoyant particle computed at each fixed position y for $R = 20$.

6. Slip velocities, angular slip velocities and lift for non-neutrally buoyant circular particles

The qualitative results which were established in § 5 hold for particles heavier and lighter than fluid. The slip velocity and angular slip velocity are positive and the angular slip velocity discrepancy changes sign across y_e, where y_e is the place where

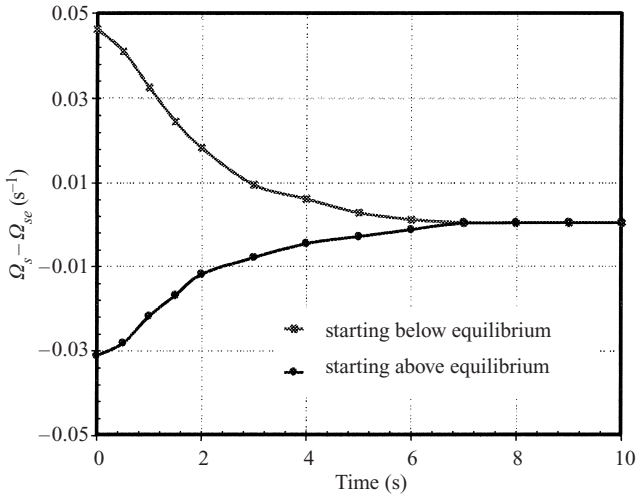

FIGURE 16. Angular slip velocity discrepancy about equilibrium for a heavier than fluid particle ($\rho_p/\rho_f = 1.01$, $R = 10$). The evolution on the angular slip velocity discrepancy is consistent with the evolution on the particle height.

the lift discrepancy

$$\mathscr{L} = L - \tfrac{1}{4}(\rho_p - \rho_f)\pi d^2 g \tag{6.1}$$

in two dimensions vanishes. For heavier than liquid particles, the position of equilibrium moves closer to the bottom wall, and for values of ρ_p/ρ_f larger than a critical value, two equilibrium heights exist (table 1).

Figures 15 and 16 are plots of the migration to equilibrium of particles starting above and below but near to equilibrium when $R = 10$ and $R_G = 9.8$ corresponding to $\rho_p/\rho_f = 1.01$. Figure 15 shows that the particles migrate to the same equilibrium whether they start from above or below the position of equilibrium. Figure 16 is a plot of the angular slip velocity discrepancy versus time; it shows that the angular slip velocity changes sign across the position of the equilibrium.

Figures 17 and 18 treat the same problem as in figures 15 and 16 but with a different initial condition. In figure 17, the particle is started from rest near the wall and the centreline, but far from equilibrium. Figure 17 show that the particle drops below equilibrium from the centreline.

Figure 19 treats the problem of slip velocity and lift for the case $R = 20$ and $R_G = 9.8$ ($\rho_p/\rho_f = 1.01$) in which there are two stable equilibrium heights (figures 3 and 5). In the dynamical simulation of a particle started from steady flow near the centreline, the particle migrates downward to the higher position of equilibrium and the angular velocity discrepancy is negative. When the particle is started from the wall it migrates upward to the lower position of equilibrium and the angular slip velocity discrepancy is positive, consistent with our hypothesis about the lift and the angular slip velocity discrepancy.

In figure 20, we consider the case of heavier than fluid particles $\rho_p/\rho_f = 1.005$ migrating at $R = 20$. For this relatively lightweight particle the equilibrium solutions are unique at $R = 20$ and the angular slip velocity discrepancy changes with the lift as the particle approaches $y_p = y_e$ from above or below.

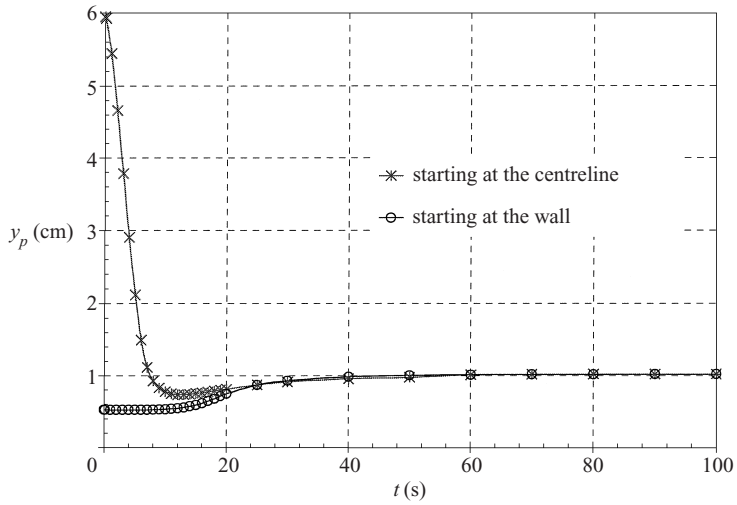

FIGURE 17. Migration from steady flow of a heavy particle $\rho_p/\rho_f = 1.01$ starting at rest near the wall and centreline at $R = 10$ ($R_G = 9.8$). The particle starting at the centreline crosses the equilibrium position and then moves upward.

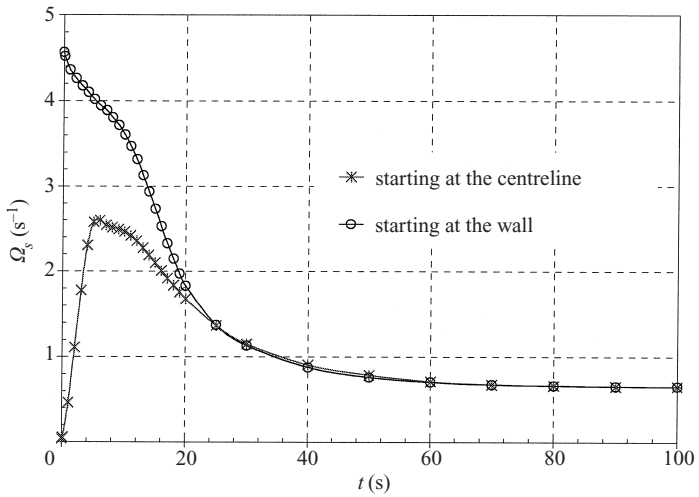

FIGURE 18. Evolution of the particle's angular slip velocity of a heavier than fluid particle $\rho_p/\rho_f = 1.01$ starting at rest near the wall and centreline at $R = 10$ and $R_G = 9.8$. For the particle starting at the centreline, the angular slip velocity function crosses the equilibrium value. When the angular slip velocity is below the equilibrium value, the particle moves downward. When the angular slip velocity is above the equilibrium value, the particle moves upward. A change in the sign of the angular slip velocity discrepancy is evident at early times when the particle falling from the centreline crosses the equilibrium; after this, both particles are below the equilibrium and have essentially the same angular slip velocity.

7. Long particle model

Joseph (2000) proposed a model problem for the velocity of a long particle in Poiseuille flow (also see Choi & Joseph 2001). We replaced the circular particle of diameter d with a long rectangle whose short side is d. The rectangle is so long that we can neglect the effects of the ends of the rectangle at sections near the rectangle centre. In that model, the long particle was assumed to be rigid, but it was noted

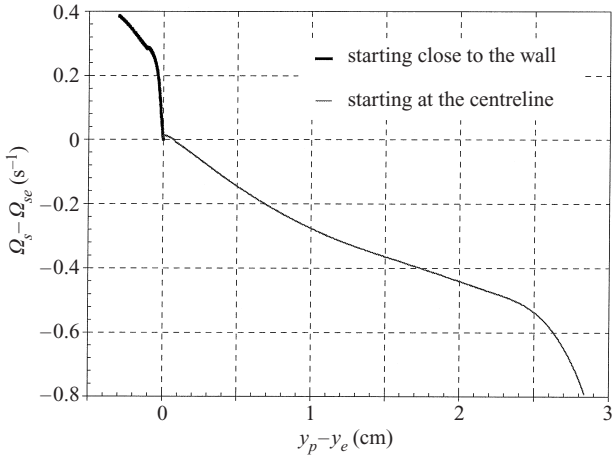

FIGURE 19. Analysis on the angular slip velocity discrepancy in the case of multiple equilibrium ($\rho_s/\rho_f = 1.01$, $R = 20$). Case (a), particle released close to the wall: ($y_p(t = 0) = 1.0$). Case (b), particle released at the centreline: ($y_p(t = 0) = 6.0$). For this data, the buoyancy force intersects the lift force at three points, and two of them yield stable solutions (figure 5). For case (a), the particle travels from a position close to the wall to the equilibrium height closer to the wall $y_e = 1.323$ cm, whereas for case (b), the particle travels from the centreline to the equilibrium height far from the wall $y_e = 3.165$ cm. The discrepancy changes sign at the equilibrium $y_p = y_e$ where the lift balances the buoyant weight.

that a more realistic model could be obtained by letting the long particle shear. We could choose this shear to be the same as the shear rate of the circular particle in the approximation in which $\Omega_p = -\frac{1}{2}\dot{\gamma}$, the diagram for this model is shown in figure 21.

The long particle model represents the constrained forward motion with y_p fixed after transients have decayed and steady flow is achieved. The model may be compared with the numerical simulation satisfying the fluid equations (3.3) with $\partial \boldsymbol{u}/\partial t = 0$, the x-component of (3.4) with $\mathrm{d}U_p/\mathrm{d}t = 0$

$$\bar{p}\boldsymbol{e}_x + \boldsymbol{e}_x \frac{1}{V_p} \oint \{-p\mathbf{1} + 2\eta \boldsymbol{D}[y]\} \cdot \boldsymbol{n}\, \mathrm{d}\Gamma = 0$$

and (3.6) with $\mathrm{d}\boldsymbol{\Omega}/\mathrm{d}t = 0$. The y-component of (3.4) gives the balance of buoyant weight and lift; the particle density enters into this balance through the buoyancy term. It follows that buoyancy and the particle density do not enter into the constrained simulations which determine the steady motion of the fluid and the forward motion of the particle, and they do not enter into the long particle model which approximates the simulation.

The model leads to an explicit expression for the particle velocity and slip velocity in which vertical migration is suppressed. Since the simulation and the model do not depend on ρ_p, there is a sense in which the results given here are universal. However, each constrained simulation is realizable for a density given by (4.1) in which the y-component of (3.4) is satisfied.

The forces acting on the long particle are the force due to pressure acting on the sides perpendicular to the flow, and the force due to shear stress acting on the sides parallel to the flow (figure 21). The former force is always positive, whereas the latter may be positive or negative depending on whether the fluid is faster than the particle or vice versa.

$$(\tau_A + \tau_B)l + (p_1 - p_2)d = 0, \tag{7.1}$$

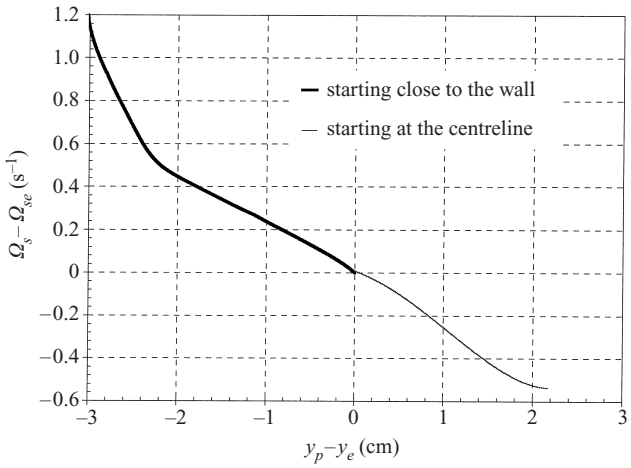

FIGURE 20. Analysis on the angular slip velocity discrepancy in the case of a unique equilibrium ($\rho_s/\rho_f = 1.005$, $R = 20$). Case (a), particle released close to the wall: ($y_p(t = 0) = 1.0$). Case (b), particle released at the centreline: ($y_p(t = 0) = 6.0$). For this data, the buoyant weight intersects the lift force at only one point (figure 5). Therefore, no matter where the particle started, it will reach the same equilibrium height at $y_e = 3.834$ cm. The discrepancy is positive if the local value is greater than the equilibrium value, and it is negative for the opposite condition. The angular slip velocity discrepancy changes its sign as the particle's height discrepancy does. *Note.* The initial condition for all the cases was as follows. First, to obtain a fully developed velocity profile, a simulation at the initial height ($y_p(t = 0) = 1.0$ or $y_p(t = 0) = 6.0$) was performed using a constrained motion on the vertical direction. Secondly, the vertical motion constraint is released, and therefore the particle travels to a preferential equilibrium height.

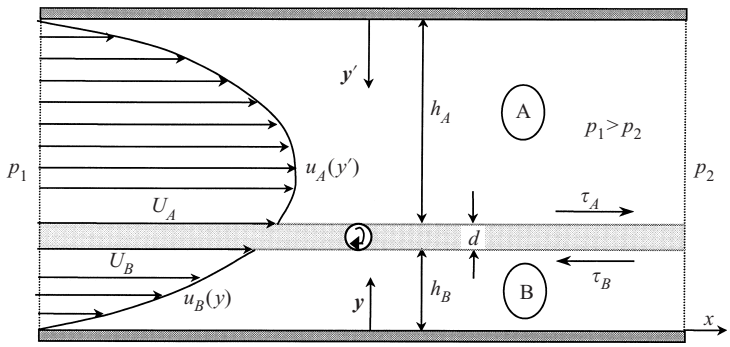

FIGURE 21. Sketch of flow field under consideration and variables involved in the long particle model. $W = h_A + h_B + d$ is the channel height.

$$\tau_A + \tau_B + \bar{p}d = 0, \quad \bar{p} = \frac{(p_1 - p_2)}{l}, \tag{7.2}$$

where the shear stresses are defined by

$$\tau_A = -\eta \frac{\mathrm{d}u_A}{\mathrm{d}y'}(h_A), \quad \tau_B = -\eta \frac{\mathrm{d}u_B}{\mathrm{d}y}(h_B). \tag{7.3}$$

The velocity profiles above and below the long particle are given by

$$u_A(y') = \frac{\bar{p}}{2\eta} y'(h_A - y') + \frac{U_A y'}{h_A}, \tag{7.4}$$

$$u_B(y) = \frac{\bar{p}}{2\eta} y(h_B - y) + \frac{U_B y}{h_B}, \tag{7.5}$$

where different velocities (U_A, U_B) were assumed for the top and bottom walls to take into account the angular speed of the circular particle. The relation between them is given by

$$U_A - U_B = \tfrac{1}{2}\dot{\gamma}(h_B + \tfrac{1}{2}d)d, \tag{7.6}$$

where $\dot{\gamma}(y)$ is the shear rate for the undisturbed flow (without the particle), given by

$$\dot{\gamma}(y) = \frac{\mathrm{d}u}{\mathrm{d}y} = \frac{\bar{p}}{2\eta}(W - 2y). \tag{7.7}$$

The shear rate on the particle's sides parallel to the flow may be evaluated from (7.4), (7.5) and (7.6),

$$\frac{\mathrm{d}u_A}{\mathrm{d}y'}(h_A) = -\frac{\bar{p}}{2\eta}h_A + \frac{U_B}{h_A} + \frac{\dot{\gamma}(h_B + \frac{1}{2}d)}{2}\frac{d}{h_A}, \tag{7.8}$$

$$\frac{\mathrm{d}u_B}{\mathrm{d}y}(h_B) = -\frac{\bar{p}}{2\eta}h_B + \frac{U_B}{h_B}. \tag{7.9}$$

Substituting, recursively, (7.8) and (7.9) into (7.3), and then the resultant equation into (7.2), we find that at the top and bottom of the long particle (diameter d):

$$U_A = \frac{(\bar{p}/\eta)(2d + h_A + h_B)h_A h_B + \dot{\gamma}(h_B + \frac{1}{2}d)h_A d}{2(h_A + h_B)}, \tag{7.10}$$

$$U_B = \frac{(\bar{p}/\eta)(2d + h_A + h_B)h_A h_B - \dot{\gamma}(h_B + \frac{1}{2}d)h_B d}{2(h_A + h_B)}. \tag{7.11}$$

The average particle velocity is:

$$U_p = \tfrac{1}{2}(U_A + U_B) = \frac{(\bar{p}/\eta)(2d + h_A + h_B)h_A h_B - \dot{\gamma}(h_B + \frac{1}{2}d)(h_B - h_A)\frac{1}{2}d}{2(h_A + h_B)}. \tag{7.12}$$

The undisturbed flow field (without the particle) can be written as:

$$u(y) = \frac{\bar{p}}{2\eta} y(W - y). \tag{7.13}$$

At the position where the centre of the particle is located ($y_p = h_B + \frac{1}{2}d$), the undisturbed fluid velocity is:

$$u(h_B + \tfrac{1}{2}d) = \frac{\bar{p}}{2\eta}(h_B + \tfrac{1}{2}d)(h_A + \tfrac{1}{2}d). \tag{7.14}$$

The particle slip velocity can be defined as:

$$U_s = u(h_B + \tfrac{1}{2}d) - U_p, \tag{7.15}$$

which can be written as:

$$U_s = \frac{(\bar{p}/\eta)[(h_A + h_B)(h_B + \frac{1}{2}d)(h_A + \frac{1}{2}d) - (2d + h_A + h_B)h_A h_B] + \dot{\gamma}(h_B + \frac{1}{2}d)(h_B - h_A)\frac{1}{2}d}{2(h_A + h_B)}. \tag{7.16}$$

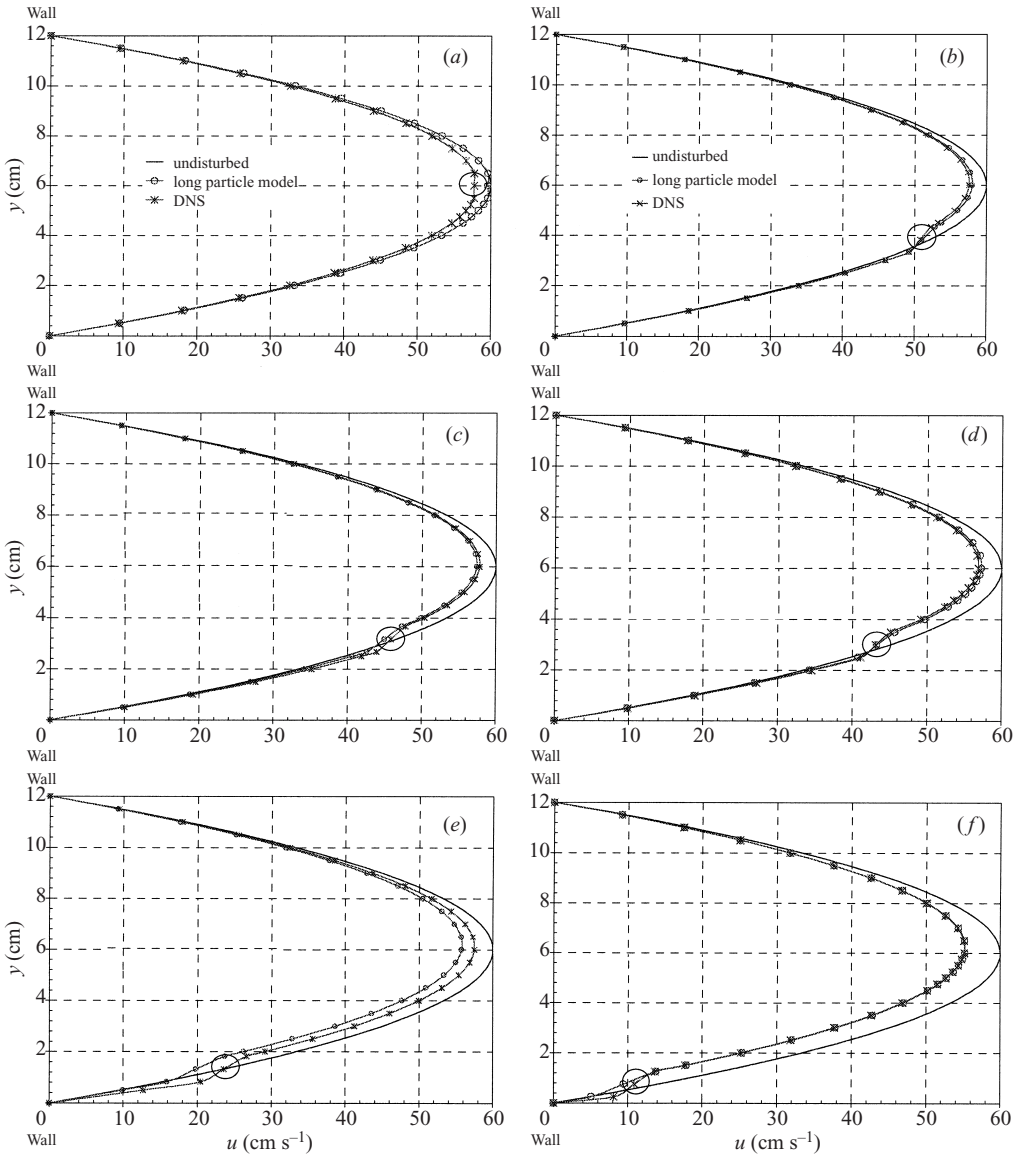

FIGURE 22. Velocity profiles through the centre y_p of a particle and the particle velocity at $R = 20$. The velocity profiles of the undisturbed flow, of the DNS simulation and the long particle model are compared: (*a*) centreline $y_p = 6.0\,\text{cm}$, (*b*) the unique equilibrium position when $\rho_p/\rho_f = 1.005$ ($y_p = 3.834\,\text{cm}$), (*c*) the higher equilibrium position when $\rho_p/\rho_f = 1.01$ ($y_p = 3.165\,\text{cm}$), (*d*) $y_p = 3.0\,\text{cm}$, (*e*) the lower equilibrium position when $\rho_p/\rho_f = 1.01$ ($y_p = 1.323\,\text{cm}$), (*f*) $y_p = 0.75\,\text{cm}$. The centreline of (*a*) is unstable.

The channel height W and the position h_A and h_B satisfy the following conditions:

$$\begin{cases} h_A = W - (h_B + d), \\ h_A + h_B = W - d, \end{cases} \qquad y_p = h_B + \tfrac{1}{2}d,$$

and the shear rate at the particle centre is

$$\dot{\gamma}(h_B + \tfrac{1}{2}d) = \frac{\bar{p}}{2\eta}(W - d - 2h_B). \tag{7.17}$$

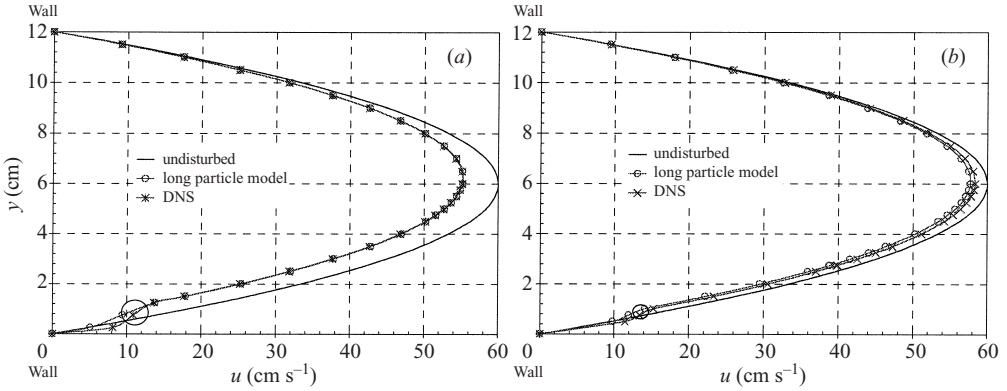

FIGURE 23. Velocity profiles at steady state on a line through the centre of a particle at $y_p = 0.75$ cm, $R = 20$. (*a*) Reference size ($d = 1.0$ cm), (*b*) small particle ($d = 0.5$ cm). As the particle is smaller, the difference between disturbed and undisturbed velocity profiles is smaller.

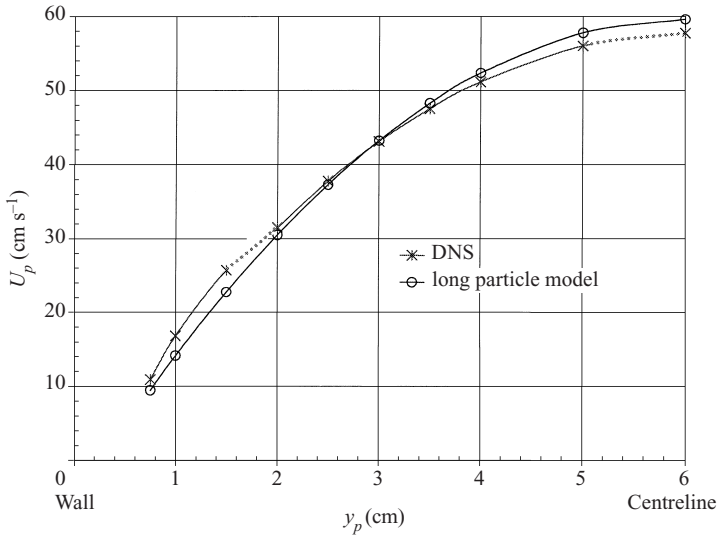

FIGURE 24. Particle velocity *vs.* particle position.

Then, the slip velocity can be simplified:

$$U_s = \frac{\bar{p}}{2\eta(h_A + h_B)}[(h_A + h_B)(h_B + \tfrac{1}{2}d)(h_A + \tfrac{1}{2}d) - (2d + h_A + h_B)h_A h_B + \tfrac{1}{2}(W - d - 2h_B)(h_B - h_A)\tfrac{1}{2}d]$$
$$= \frac{\bar{p}}{2\eta(W - d)}[d(\tfrac{1}{2}W - y_p)^2 + \tfrac{1}{4}d^2(W - d)] \geqslant 0 \qquad (7.18)$$

when $d \to 0$, we find $U_s \to 0$.

A comparison of the long particle model with DNS for a circular particle is given in figures 22 and 23. In these constrained simulations we fix the y position of the particle and compute the dynamic evolution to equilibrium at $R = 20$. The diameter of the particle in figure 22 is 1 cm and in 23 it is 0.5 cm. The profiles in the figures are at equilibrium and on a cross-section through the centre of the particle. The agreement

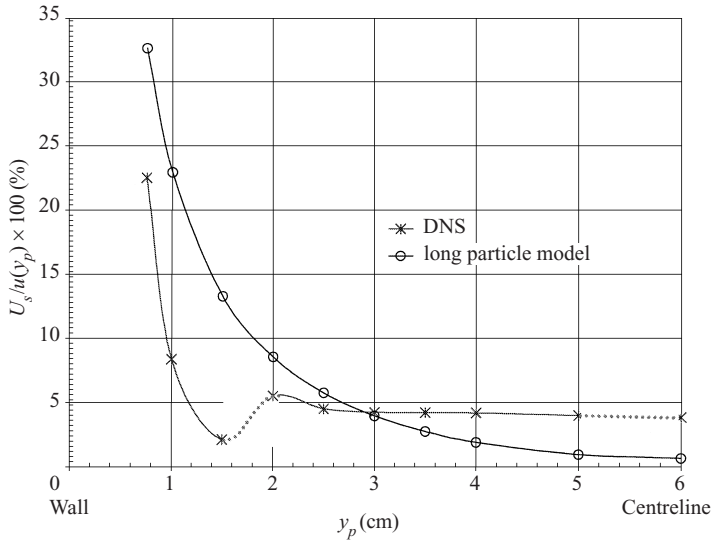

FIGURE 25. Slip velocity/fluid velocity ratio *vs.* particle position at $R = 20$. Slip velocity evaluated using DNS results *vs.* slip velocity in the long particle model. These are relative values of the slip velocity, U_s with respect to the fluid velocity on the undisturbed flow at the particle centre $u(y_p)$. The largest discrepancy is at about $\frac{1}{4}$ the distance from the wall to the centreline.

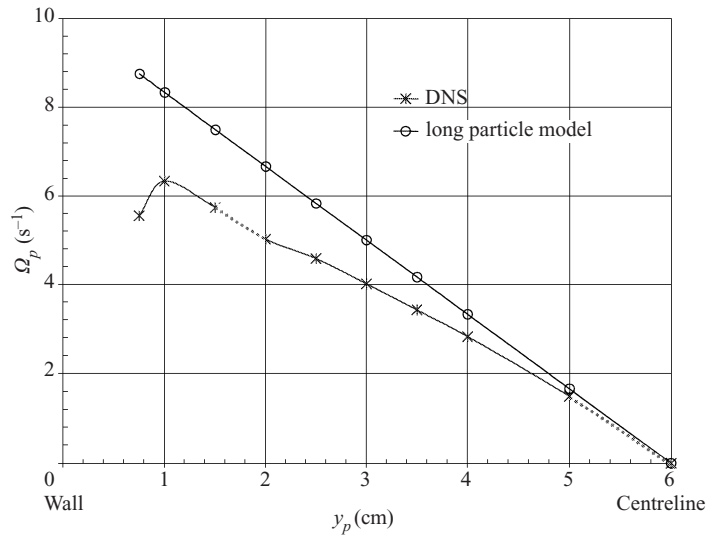

FIGURE 26. Particle angular velocity, Ω_p at $R = 20$. the angular velocity of the particle is approximated in the long particle model as minus half the value of the shear rate on the undisturbed flow evaluated at the particle centre position $\Omega_p|_{LPM} = -\frac{1}{2}\dot{\gamma}(y_p)$.

is better than might have been anticipated, given the severe assumptions required in the model. The agreement is quite good away from the centreline, even close to the wall. Equations (7.2)–(7.6) can be recommended for an analytical approximation for the velocity of a circular particle in Poiseuille flow.

In figure 24, we compare the particle velocity from the simulation with the long particle model. In figure 25, we compare the slip velocity, and in figure 26 we show how nearly the particles angular velocity is given by $(-\frac{1}{2}\dot{\gamma})$.

8. Summary and conclusion

The lift and migration of neutrally buoyant and heavier-than-liquid circular particles in a plane Poiseuille flow was studied using direct numerical simulation. The study looks at the relation of slip velocity and angular slip velocity to lift and migration. No matter where the neutrally buoyant particle is released, it will migrate to a unique equilibrium height and move forward with a unique steady particle velocity and rotate with unique steady angular velocity. Neutrally buoyant particles migrate to a radius which can be called the 'Segré–Silberberg' radius. This radius is a reference; heavier-than-liquid particles also migrate to an equilibrium radius that is close to the Segré–Silberberg radius if the particle density is close to the fluid density. The particles migrate to an equilibrium position y_e with shear rate $\dot{\gamma}_e$ such that the local fluid rotation $(-\frac{1}{2}\dot{\gamma}_e)$ is slightly greater than the particle angular velocity Ω_p. The angular slip velocity, $\Omega_s = \Omega_p + \frac{1}{2}\dot{\gamma}_e$ is always positive, but at equilibrium it is very small; $\Omega_p \approx -\frac{1}{2}\dot{\gamma}_e$ can be proposed as an approximation. The slip velocity at equilibrium $U_s = U_{fe} - U_p$ is alway positive and slowly varying.

Since the shear rate and slip velocities are one-signed they do not explain why the lift changes sign across the equilibrium radius. We found that the quantity which does change sign at y_e is the angular slip velocity discrepancy; the angular slip velocity minus the equilibrium angular slip velocity $\Omega_s - \Omega_{se}$. $\Omega_s - \Omega_{se} > 0$ when $y < y_e$ and $\Omega_s - \Omega_{se} < 0$ when $y > y_e$. The adjustment of the angular slip velocity of a free particle is very critical to lift. We might think of the angular slip velocity discrepancy as a shear flow analogue to the circulation in aerodynamic lift.

We derived a shear version of our long particle model. The long particle model arises when the circular particle is replaced with a long rectangle of the same diameter as the circle, but so long that we may neglect end effects. In the shear version, we allow the rectangle to shear at the rate $(-\frac{1}{2}\dot{\gamma})$ of the local rotation. Using this model, we can find explicit expressions for the fluid rotation in which the velocity on either side of the long particle is matched by the fluid velocity; then we satisfy the particle equation of motion in which the shear stress force balances the pressure drop force. This leads to explicit expression for the velocity of the particle (7.12) and the slip velocity (7.16) that is always positive. The shear version of the long particle model is in good agreement with the results of numerical computation of the motion of a free circular particle at points of stable equilibrium, both with respect to the particle velocity and the fluid velocity on the cross-section containing the centre of the circular particle.

The results given in this paper are for two dimensions. It remains to be seen how such results carry over to three dimensions. We note that the celebrated lift formula $\rho U\Gamma$ is a two-dimensional result.

This work was partially supported by the National Science Foundation KDI/New Computational Challenge grant (NSF/CTS-98-73236); by the US Army, Mathematics; by the DOE, Department of Basic Energy Sciences; by a grant from the Schlumberger foundation; from STIM-LAB Inc.; and by the Minnesota Supercomputer Institute.

REFERENCES

Asmolov, E. S. 1999 The inertial lift on a spherical particle in a plane Poiseuille flow at large channel Reynolds number. *J. Fluid Mech.* **381**, 63–87.

Auton, T. R. 1987 The lift force on a spherical body in a rotational flow. *J. Fluid Mech.* **183**, 199–218.

Cherukat, P., McLaughlin, J. B. & Dandy, D. S. 1999 A computational study of the inertial lift on a sphere in a linear shear flow field. *Intl J. Multiphase Flow* **25**, 15–33.

Choi, H. G. & Joseph, D. D. 2001 Fluidization by lift of 300 circular particles in plane Poiseuille flow by direct numerical simulation. *J. Fluid Mech.* **438**, 101–128.

Drew, D. A. & Passman, S. 1999 *Theory of Multicomponent Fluids*. Springer.

Feng, J., Hu, H. H. & Joseph, D. D. 1994 Direct simulation of initial values problems for the motion of solid bodies in a Newtonian fluid. Part 2. Couette and Poiseuille flows. *J. Fluid Mech.* **277**, 271–301.

Ho, B. P. & Leal, L. G. 1974 Inertial migration of rigid spheres in two-dimensional unidirectional flow. *J. Fluid Mech.* **65**, 365–400.

Joseph, D. D. 2000 Interrogation of direct numerical simulation of solid–liquid flow, to appear, see also http://www.aem.umn.edu/people/faculty/joseph/interrogation.html.

Kurose, R. & Komori, S. 1999 Drag and lift forces on a rotating sphere in a linear shear flow. *J. Fluid Mech.* **384**, 183–206.

McLaughlin, J. B. 1991 Inertial migration of a small sphere in linear shear flows. *J. Fluid Mech.* **224**, 261–274.

Mortazavi, S. & Tryggvason, G. 2000 A numerical study of the motion of drops in Poiseuille flow. Part 1. Lateral migration of one drop. *J. Fluid Mech.* **411**, 325–350.

Patankar, N., Huang, P. Y., Ko, T. & Joseph, D. D. 2001 Lift-off of a single particle in Newtonian and viscoelastic fluids by direct numerical simulation. *J. Fluid Mech.* **438**, 67–100.

Saffman, P. G. 1965 The lift on a small sphere in a slow shear flow. *J. Fluid Mech.* **22**, 385–400; and Corrigendum, *J. Fluid Mech.* **31**, 624 (1968).

Schonberg, J. A. & Hinch, E. J. 1989 Inertial migration of a sphere in Poiseuille flow. *J. Fluid Mech.* **203**, 517–524.

Segré, G. & Silberberg, A. 1961 Radial Poiseuille flow of suspensions. *Nature* **189**, 209.

Segré, G. & Silberberg, A. 1962 Behaviour of macroscopic rigid spheres in Poiseuille flow. Part 1. *J. Fluid Mech.* **14**, 115–135.

Vasseur, P. & Cox, R. G. 1976 The lateral migration of a spherical particle in two-dimensional shear flow. *J. Fluid Mech.* **78**, 385–413.

Zhao, Y., Sharp, M. K. & James, K. 1998 Finite-element analysis of transverse lift on circular cylinder in 2D channel flow. *J. Engng Mech.* **124**, 1151–1164.